STEWARD-1047
Fermilab Library
0 1160 0015465 2
CUTE TO
NAME LOCATION
RETURN TO FERMI LIBRARY

PREPRINTS

of the

STEWARD OBSERVATORY

THE UNIVERSITY OF ARIZONA
TUCSON, ARIZONA 85721 U.S.A.

No. 1047

ADAPTIVE OPTICS AT THE MULTIPLE MIRROR TELESCOPE

M. Lloyd-Hart, P. Wizinowich*, R. Angel, B. McLeod, D. McCarthy, D. Colucci,
R. Dekany and D.Wittman

Steward Observatory, University of Arizona, Tucson, Arizona 85721
*Currently at the W. M. Keck Observatory, P.O. Box 220, Kamuela, Hawaii 96743

Proceedings of the Laser Guide Star Adaptive Optics Workshop
Phillips Laboratory
Kirtland Air Force Base
Albuquerque, New Mexico
March 10-12, 1992

FERMILAB
MAY 11 1992
LIBRARY

Adaptive optics at the Multiple Mirror Telescope

M. Lloyd-Hart, P. Wizinowich*, R. Angel, B. McLeod, D. McCarthy, D. Colucci, R. Dekany, & D. Wittman

Steward Observatory, University of Arizona, Tucson, AZ 85721
*Currently at the W.M. Keck Observatory, P.O. Box 220, Kamuela, HI 96743

ABSTRACT

The next generation of 6 to 10 m class telescopes is being planned to include the capability for adaptive wavefront correction. The Multiple Mirror Telescope (MMT) with its 7 m baseline, provides an ideal testbed for novel techniques of adaptive optics at full scale. Using a new instrument based on a six segment adaptive mirror, a number of wavefront sensing algorithms including an artificial neural network have been implemented to demonstrate the high resolution imaging capability of the telescope. These algorithms rely on a freely-available property of starlight, namely its coherence over large scales, to sense directly atmospheric and instrumental phase errors across large distances. In this paper, we report results obtained so far with resolutions between 0.08 and 0.3 arcseconds at 2.2 μm wavelength. We also show data indicating that at the level of 0.1 arcsec imaging in good seeing, the isoplanatic patch at this wavelength is at least 20 arcsec across.

1. INTRODUCTION AND INSTRUMENT DESCRIPTION

The adaptive optics group at Steward Observatory has been active now for about two years. This paper is intended as a summary of the different approaches we have begun to explore for adaptive wavefront control at large astronomical telescopes. We have concentrated our effort thus far on the MMT, located on Mt. Hopkins in Arizona. The intention has been to develop techniques which will be applicable to future telescopes, and to begin a program of scientific research in astronomy, taking advantage of diffraction-limited imaging with the MMT in the near infrared.

To exploit the full resolution and deep imaging capabilities of present and future generations of large telescopes, adaptive wavefront correction is essential. Imaging at the diffraction limit requires that the shape of the wavefront be known to a small fraction of a wave on scales from the atmospheric correlation length r_0 up to the longest baseline of the telescope. Large scale phase distortion is especially important since it accounts for a major portion of the turbulence power spectrum. An objective of our adaptive optics research at the MMT is to take advantage of the 7 m baseline to investigate ways to reconstruct phase errors accurately over large scales. Under good seeing conditions, correction of tilt and piston error across each of the six 1.8 m diameter segments of the MMT is sufficient to recover diffraction-limited resolution at 2.2 μm of 0.06 arcsec full width at half maximum[1], with high Strehl ratio (the ratio of peak intensity to that of the diffraction-limited image).

Phase differences across large distances are generally obtained by integrating local

slopes measured with r_0 sized subapertures. Methods based on this approach have been extensively developed to work in adaptive optics systems, particularly those using laser beacons[2,3], which must tolerate a source diffuse over an arcsecond or more. These techniques inherently introduce errors since they assume that the wavefront is smooth on scales smaller than the subaperture, which is not the case for a true atmospheric wavefront. However, if a spatially coherent source such as a star is used as the wavefront reference, large scale phase errors can be measured directly with high accuracy from interference in the far-field image plane. The global shape of the wavefront is measured directly from focal plane images showing the effects of interference across the full aperture. This approach is particularly valuable if the wavefront has discontinuities, as in segmented or array telescopes. We have been experimenting with techniques which derive the required phases either from direct analysis of the interference[4,5], or from the Fourier transform of the short exposure image.

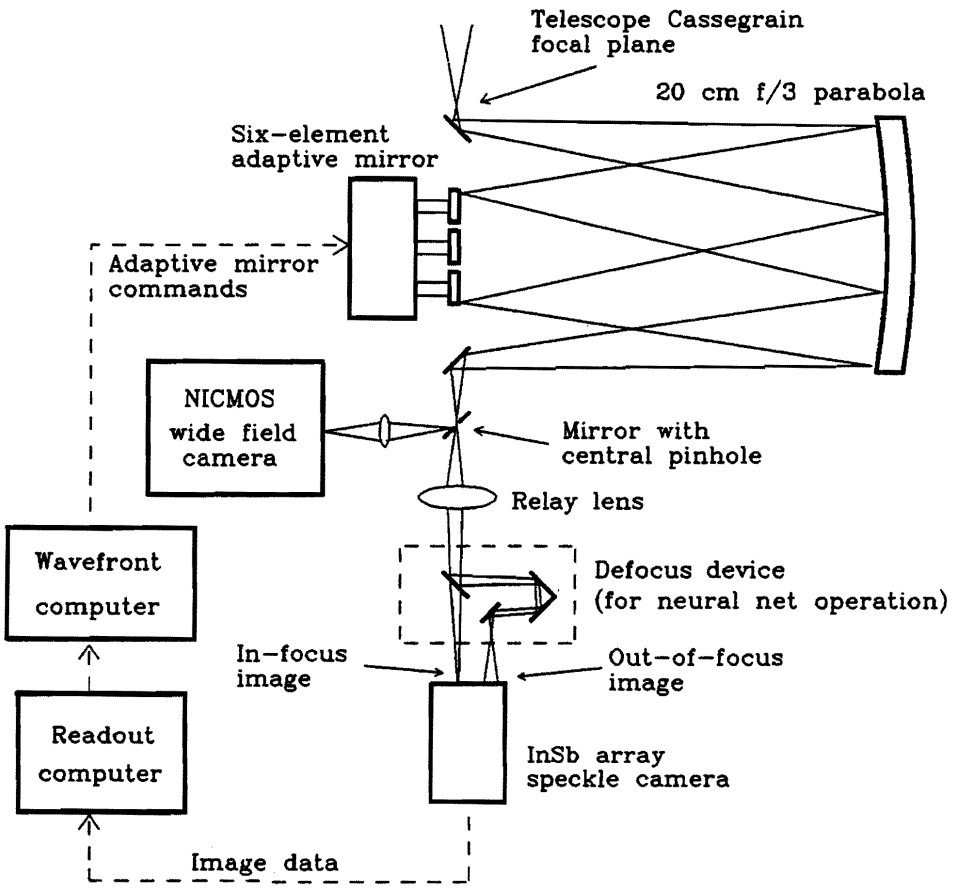

Figure 1. The adaptive instrument is mounted at the Cassegrain focus of the MMT. The adaptive mirror is placed close to a re-imaged pupil, in the focal plane of a parabola which collimates the beam from the telescope, and reflects it after correction to a second focus. Light from the field around the reference star is reflected to a wide-field integrating camera, while light from the star is transmitted to a relay lens which magnifies the beam from f/8.39 to f/45. A computer reads the infrared camera and transmits the images to the wavefront computer, which closes the loop by controlling the adaptive mirror.

The complete instrument, shown schematically in figure 1, is described in detail elsewhere[6]. In brief, the stellar image formed at the telescope's prime focus is relayed at unit magnification to a second focus via the segmented adaptive mirror, positioned close to an image of the pupil. The corrected field is reflected off a mirror with a central hole to a 128 square NICMOS2 HgCdTe array. The image of the reference star, transmitted through the hole, is magnified by a lens onto a 62×58 pixel indium antimonide infrared array[7], at a plate scale of 0.04 arcsec/pixel. For operation of the neural network wavefront sensor, additional optics are inserted just ahead of the array which generate simultaneous in- and out-of-focus images, placed side by side on the detector. The additional defocussed image is required for an unambiguous determination of the shape of the wavefront.

To be effective, the correction cycle which includes integration of an image, readout of the infrared camera, processing by the wavefront computer, and adjustment of the adaptive mirror, must be very fast, no more than about 20 ms for good correction at 2 μm. Because the wavefront reconstruction algorithms are extremely computationally intensive, and are essentially parallel in nature, we decided to base the wavefront computer on an array of transputers which runs at 25 Mflops, fast enough to compute the wavefront parameters in a few milliseconds. We use 16 T800-25 transputer modules, manufactured by Inmos Inc., running at 25 MHz, and an additional 4 T800-20 chips which run at 20 MHz.

The remainder of this paper describes work on three different approaches to wavefront control which have been explored with the MMT adaptive system. All the results presented here were obtained in the K photometric band (2.2 μm centre wavelength with 0.42 μm bandpass).

2. BRIGHT PIXEL TRACKING

In the regime of seeing where $D/r_0 < 2.7$, where D is the aperture diameter, telescope images are characterised by a single bright speckle of diffraction-limited size which moves in the image plane as the wavefront tilt changes[1]. In terms of the wavefront, after removal of the global tilt, the remaining r.m.s. phase error is < 1 radian. By tracking the speckle with a tip/tilt steering mirror, one can obtain integrated images with a strong diffraction-limited component. This technique is similar to the post-processing method of simple shift-and-add[8], except that an integrated image with the NICMOS camera may be obtained in the full corrected field of view by a single long exposure rather than a series of short-exposure specklegrams. The integrated image then has the improved noise characteristics of the long exposure.

As an initial test to demonstrate the effectiveness of the new instrument, we took images of the binary star γ^2 Andromedae. These stars, separated at present by 0.56 arcsec, form part of a triple system, with the primary, γ^1 Andromedae, about 11 arcsec away. The system is an excellent testing ground for near infrared adaptive optics. By tracking the image of the primary, dramatic improvement is seen in the image of the secondary and tertiary components.

Figure 2 shows two five second exposures of γ^2 And taken with the NICMOS2

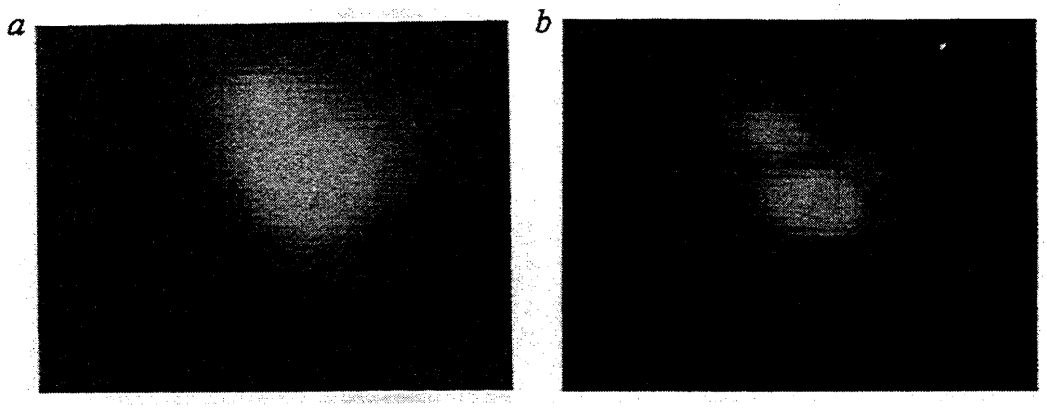

Figure 2. K band images of the star γ^2 And, recorded with 5 s exposures on the NICMOS2 camera using a single MMT mirror. *a* The uncorrected image; *b* the result when the image of γ^1 And, 11 arcsec away, was stabilised with a rapid tip/tilt mirror tracking the brightest speckle. The separation of the two stars is 0.56 arcsec.

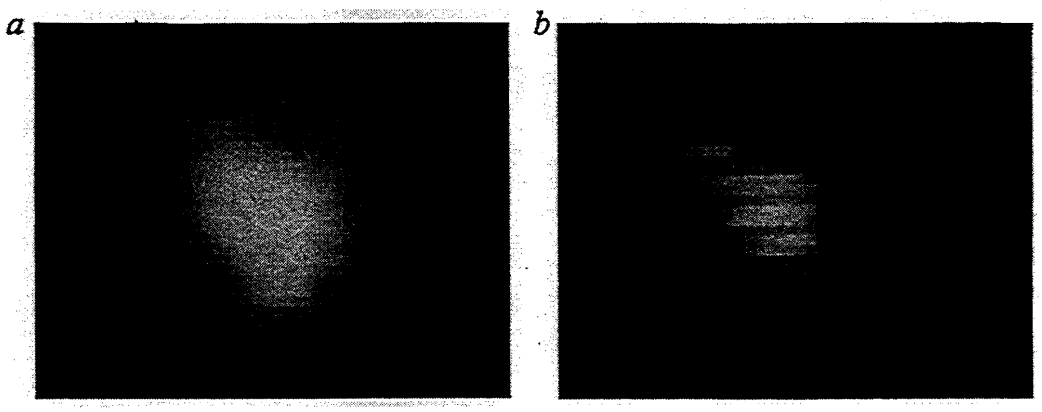

Figure 3. Images of γ^2 And taken with two coherently phased mirrors of the MMT. *a* The uncorrected image; *b* when the image of the primary was stabilised with the bright speckle tracking algorithm, interference fringes appear in both components of γ^2 And.

camera, with just one of the six telescope mirrors. No tracking was used for figure 2*a*, and the result is a seeing-limited image with FWHM of 0.45 arcsec. When bright speckle tracking was used to stabilise the image of γ^1 And on the InSb camera at a closed-loop correction rate of 75 Hz, figure 2*b*, the binary is much better resolved, with a FWHM of 0.31 arcsec in the vertical direction. The corrected images are slightly elongated because the pupil mask used in this experiment projected to an ellipse on the camera, with a major axis of 1.63 m, giving a diffraction limit of 0.28 arcsec.

In an otherwise identical experiment, two coherently phased mirrors of the telescope were used. Each aperture was 1.63 m in diameter, with a centre-to-centre separation of 2.88 m. The instantaneous image shows Young's interference fringes, and the tracking algorithm steers the combined image on the basis of the brightest fringe. In the uncorrected case, figure 3*a*, the effects of interference have been completely washed out by atmospheric

phase fluctuations, but with adaptive control applied, figure 3*b*, both components of γ^2 And show strong fringes with a diffraction-limited FWHM of 0.08 arcsec, and a contrast of about 25%. This experiment serves as an excellent demonstration that the isoplanatic patch for full correction at 2 μm in good seeing is at least 20 arcsec in diameter.

3. ARTIFICIAL NEURAL NETWORK

While simple tip/tilt control can produce excellent results in good seeing, it breaks down rapidly for $D/r_0 > 2.7$. In this regime, snapshot images no longer consist of a single strong speckle; there are multiple bright speckles and the tracking algorithm frequently chops between speckles, thereby blurring the integrated image. A more sophisticated algorithm is required.

One such method, which uses a trained artificial neural network, has been developed by Sandler *et al*[9]. Star images reduced off-line were shown to yield aberrations in agreement with those from a conventional pupil plane wavefront sensor. We have shown by computer simulation that the method is sensitive to the interference effects and will work in the limit of infrared star images dominated by speckle structure, and with telescope arrays as well as filled apertures[1].

We have successfully implemented a neural network in real time at the telescope[5]. In this experiment, the telescope pupil was the same as for the two beam tracking result of section 2. Five degrees of freedom are controlled by the net. These are the mean slopes across each of the two apertures, and the average phase error between them. Input to the net consists of two focal plane images of an unresolved star, one in focus and the other slightly out of focus. The signals at the pixels, which form the input vector to the neural net, are normalised by the total energy in the in-focus image, which makes the net insensitive to changes in the flux from the star. The network has 300 inputs, each coupled to every one of 36 hidden nodes through a matrix with 300×36 elements. A 36×6 element matrix connects the hidden nodes to the six outputs, four of which are the tilt components of the wavefront segments. The remaining two output nodes represent the sine and cosine of the phase difference between the apertures. Readout, image processing, and correction of the adaptive mirror requires 10 ms in total, which together with the 10 ms exposure time yields a closed-loop correction rate of 50 Hz. The non-destructive readout mode used requires that the camera be reset every few frames (six in the present case). This takes an extra 6.8 ms, leading to short gaps in the flow of data.

The neural net has a multiple-perceptron architecture[10], and was trained using the back-propagation algorithm[11]. Training, which took about 25 minutes, was done in the laboratory with 30,000 image pairs generated at 20 Hz by the adaptive instrument itself. An artificial star produced by a tungsten filament lamp illuminating a 10 μm pinhole was used, and distorted images were generated by deliberately misaligning the adaptive mirror elements by known random amounts. After training, the net outputs yielded very accurately the corrections needed to cancel any random wavefront errors introduced in this way. Images formed by averaging several hundred individual frames after correction by the net show Strehl ratios in excess of 0.95 [12]. While the training images have similar distortion to

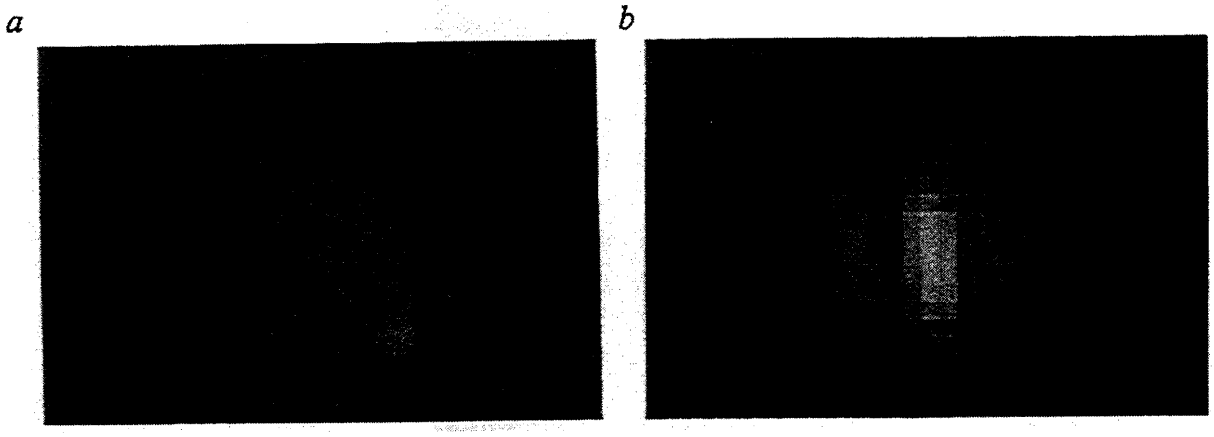

Figure 4. Two 10 s exposures of the star ψ Pegasi obtained by adding 1,000 10 ms snapshots taken at 100 Hz using two adjacent MMT mirrors. *a* An uncorrected image, FWHM = 0.62 arcsec, Strehl ratio = 0.15; *b* an image recorded immediately afterwards in which the neural network was controlling the adaptive mirror. The image shows high contrast interference fringes with a Strehl ratio = 0.27. Resolution across the fringes is 0.1 arcsec.

that seen in stellar images, they lack the fine-scale aberration produced by the atmosphere, and the known residual telescope aberration arising from the three hard points supporting each primary mirror. Experience has shown that a net trained without these effects may be useless. Additional training was therefore performed with 10,000 computer-simulated images which included them.

During a run at the MMT in September 1991, the net was successful in significantly reducing the atmospheric phase fluctuations from images of the star ψ Pegasi, which has a K magnitude of +0.03. In figure 4, we show two 10 s exposures, each obtained by adding 1,000 consecutive 10 ms frames. No correction was applied during the first exposure (figure 4*a*), and the result is an image with seeing-limited resolution of 0.62 arcsec FWHM and a Strehl ratio of 0.15. In this image, the interference fringes have been completely washed out by atmospheric phase fluctuations. A second exposure (figure 4*b*) was taken immediately after the first, during which the two corresponding adaptive mirror segments were under the control of the neural network. This image exhibits strong interference fringes with a FWHM of 0.1 arcsec and a significant reduction in the overall width from the wavefront

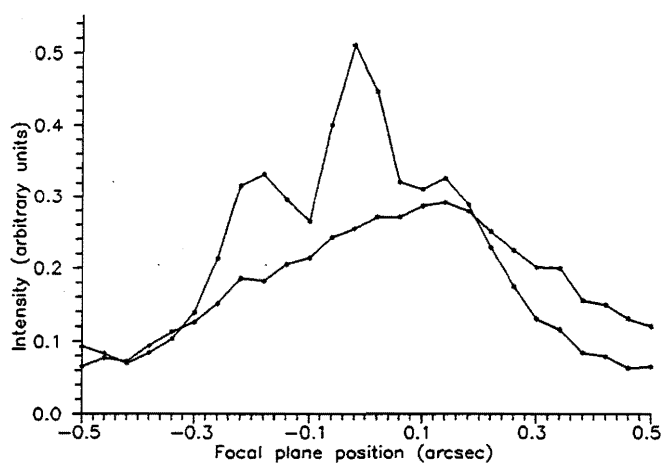

Figure 5. Horizontal cuts through the brightest pixels of the images in figure 4. The FWHM is reduced from 0.68 to 0.45 arcsec.

slope control. The Strehl ratio of the corrected image is 0.27.

The improvement in Strehl ratio and resolution can be seen clearly in figure 5, which shows linear cuts through the brightest pixels of the images in figure 4, across the fringes. The overall FWHM of the uncorrected image in this direction is 0.68 arcsec, which includes 0.06 arcsec residual stacking error in the two beams. With the net running, this was reduced to 0.45 arcsec. The success of the neural net in correcting for piston errors can be seen in figure 6, which plots the mean phase difference between the apertures for the two sets of exposures. This is found by examining the Fourier transform of each 10 ms snapshot to find the phase of the spatial frequency corresponding to the baseline separation. The mean square phase has been improved from 29.9 rad^2 to 2.87 rad^2. The uncorrected mean square

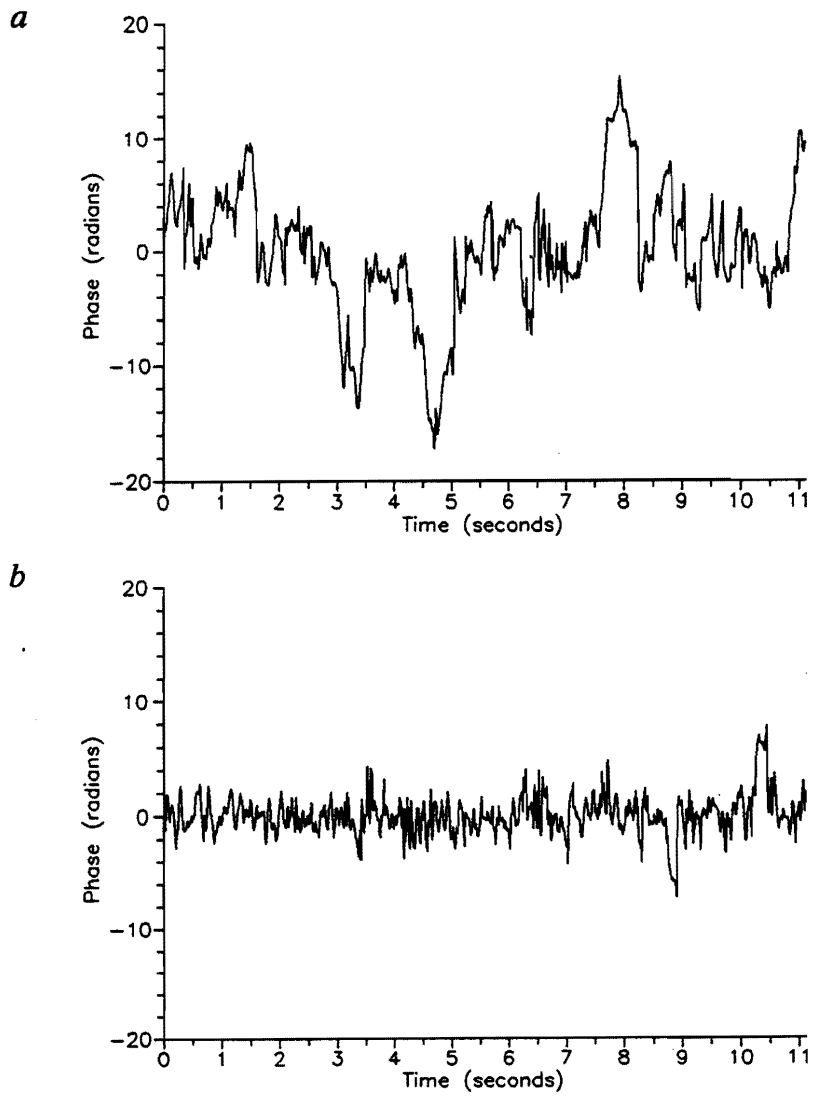

Figure 6. Relative phase between the two apertures as a function of time for the uncorrected image, *a*, and corrected image, *b*. Phase is measured by looking at the appropriate component in the Fourier transform of each 10 ms frame. The mean square values are 29.9 rad^2 and 2.87 rad^2 for *a* and *b* respectively.

phase σ^2 gives a direct measure of the atmospheric spatial structure function at separation D = 2.88 m. From the defining relation (the Kolmogorov structure function)

$$\sigma^2 = 6.88\left(\frac{D}{r_0}\right)^{\frac{5}{3}} \tag{1}$$

we find these data correspond to a correlation length, r_0 = 1.19 m at 2.2 μm wavelength.

An ideal adaptive corrector which removes all aberration would recover fringes with a Strehl ratio S = 1, in a diffraction envelope of FWHM λ/D = 2.2 μm/1.63 m = 0.28 arcsec. The experiment achieved S = 0.27 and a FWHM of 0.45 arcsec. The reduction in Strehl ratio and increase in FWHM are due to uncorrected fine-scale atmospheric errors, residual errors in alignment and surface quality of the telescope mirrors[13], the 20 ms time delay between sensing and correction, and inadequacies in the training data, which do not exactly simulate the character of the real images.

Our expectation is that a net trained on real telescope images will perform with the very high accuracy achieved in the laboratory, provided that the corresponding wavefronts are accurately characterised. We plan further experiments in which independent sensing of atmospheric wavefront errors, for example from pupil plane slope measurements and focal plane interferometry, is used to refine the net coefficients on-line at the telescope. In this process, the rapid change in the wavefront will be favorable, allowing us to obtain a complete training set of 50,000 image pairs in about 40 minutes. Currently, effort is being devoted to training a neural network to correct all six apertures of the MMT, which will allow diffraction-limited resolution of 0.06 arcsec FWHM to be achieved.

4. HYBRID PISTON AND TIP/TILT CORRECTION

We have begun to explore a new method for adaptive correction at the MMT. This is a hybrid approach in which the wavefront tilts across each of the six apertures are removed by an image motion sensor, based on a small format, low noise CCD. The remaining piston errors are found from the Fourier transform of the far-field infrared image. In the Fourier plane, the sinusoidal interference term from each pair of apertures in the pupil defines a point. The phase at that point is exactly the mean OPD or piston error between the apertures, introduced by the atmosphere and the instrument.

4.1 Fourier piston retrieval

The technique is not applicable directly to the full MMT aperture, because multiple redundancies in the pupil make it impossible to extract all the piston errors without ambiguity. However, simulations with a pupil consisting of five MMT mirrors have shown that the Fourier plane technique is very powerful. In conditions of moderately good seeing, where r_0 = 1.1 m, for a star of K magnitude 5 and a detector such as our InSb array with 300 electrons per pixel r.m.s. readout noise, piston correction alone is sufficient to recover a high contrast diffraction-limited image with a Strehl ratio of around 0.2 (figure 7).

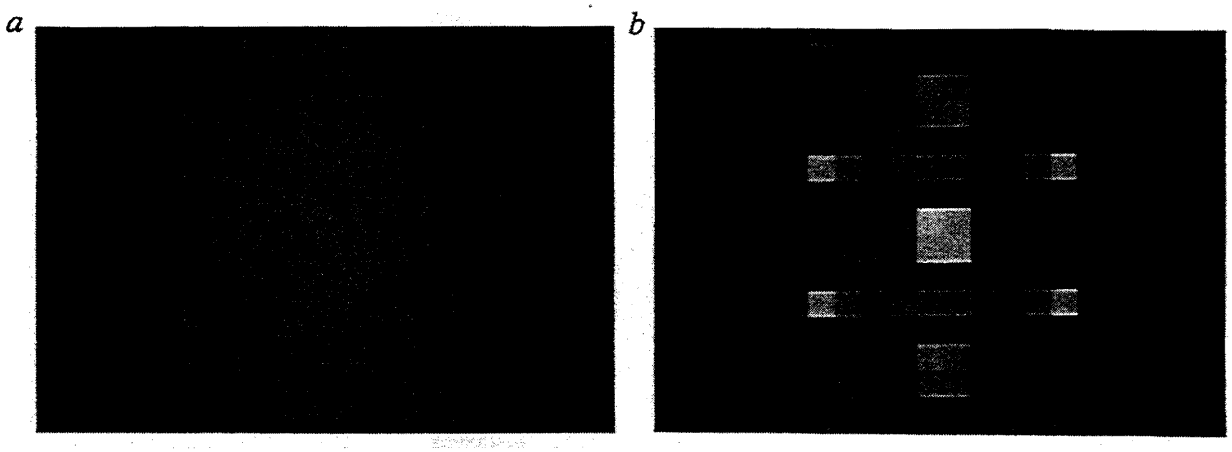

Figure 7. Simulated correction using Fourier transform piston retrieval for a 5th magnitude star, using a detector with r.m.s. noise of 300 electrons per pixel. No tip/tilt control was used. *a* An uncorrected image with FWHM = 0.52 arcsec; *b* correction of piston alone restores a diffraction-limited component with a Strehl ratio of 0.22.

Simultaneous tip/tilt correction improves the Strehl ratio to about 0.75 [12]. Perfect tip, tilt, and piston sensors would achieve a Strehl ratio of 0.76, the remaining beam degradation being due to uncorrected high spatial frequency aberration.

We have implemented the Fourier plane piston reconstructor on the transputers. Initial tests will be conducted in May 1992 beginning with the simple case of a two mirror pupil, with the same geometry as in the previous sections. If this is successful, we will attempt to stabilise the phase across the five beam pupil.

4.2 Preliminary tests with the CCD tip/tilt controller

As illustrated by the computer simulations, the Strehl ratio of the final integrated image is greatly improved if a separate tip/tilt control loop keeps all the beams stacked in the infrared focal plane. We plan to implement an image motion sensor using a 24×48 frame transfer CCD, running at about 250 Hz frame rate. Since both visible and infrared wavelengths will be used to derive wavefront corrections, the signal-to-noise ratio of the system as a whole will be fundamentally improved.

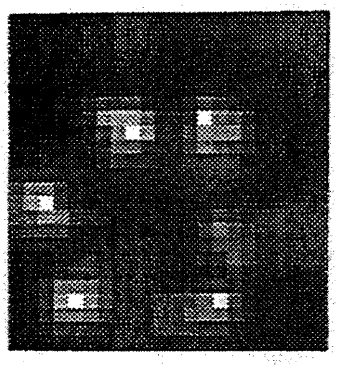

Figure 8. The six separated beams from the MMT fall onto the CCD, which allows the position of each image, and hence the corresponding wavefront tilt to be determined.

During the January run, the applicability of the CCD to an infrared adaptive system was tested by taking measurements of stellar image motion simultaneously with the CCD and the InSb camera. Figure 8 shows an example of a 26 ms exposure of a star, with the six apertures imaged onto separate parts of the active area at a plate scale of 0.25 arcsec/pixel. Figure 9 shows plots of the motion, and the computed difference for the elevation axis of a single telescope. It is clear that tracking the visible centroid is an excellent way to stabilise the infrared motion; the r.m.s. value of the difference is only 0.015 arcsec. With the high read rate and low noise (3 electrons per pixel r.m.s. is expected), this result shows that the CCD is ideally suited for an infrared adaptive optics system.

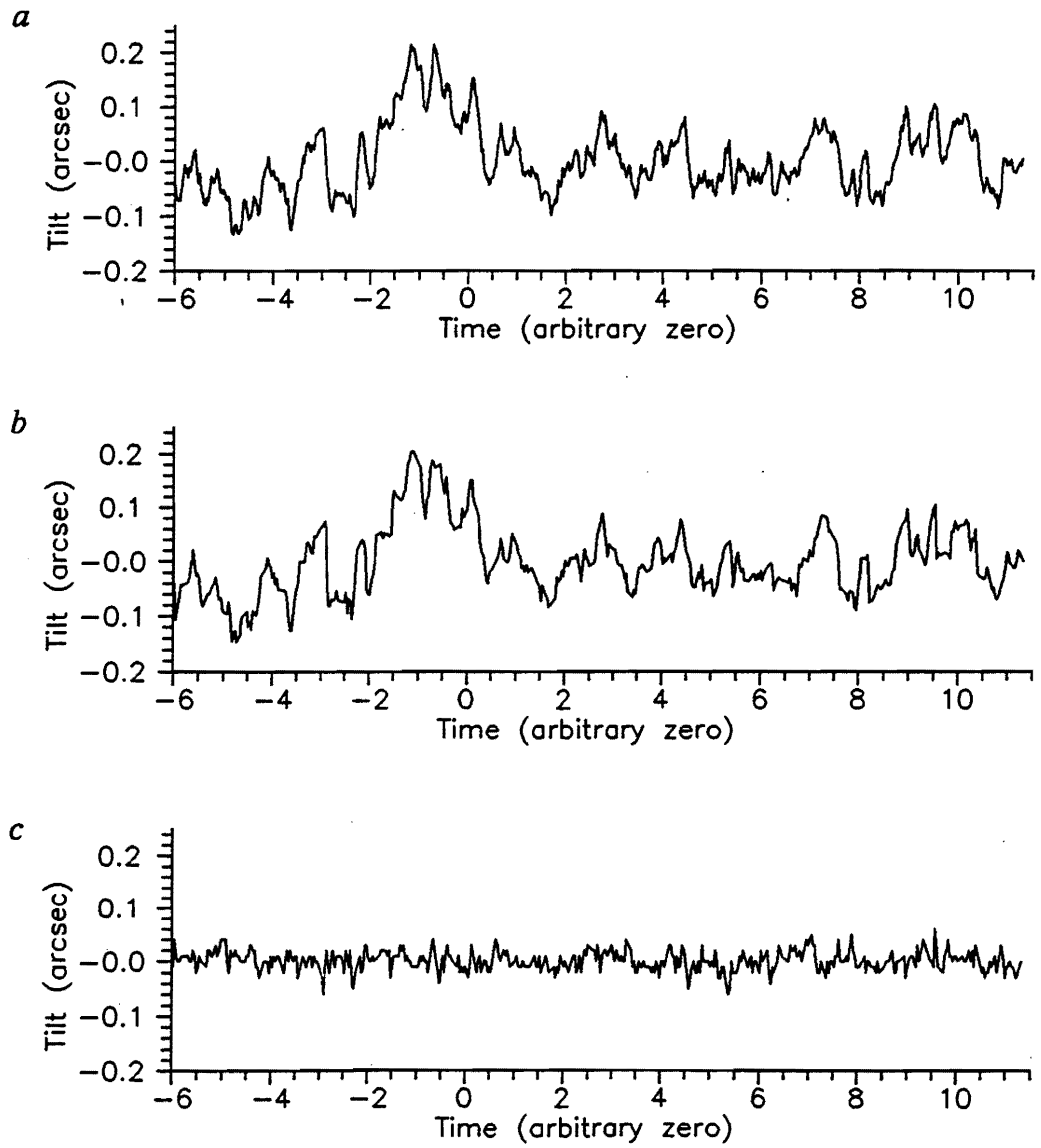

Figure 9. Image motion of a star measured simultaneously by *a* the 24×48 CCD in the visible, and *b* the InSb infrared camera at 2.2 μm. The r.m.s. value of the difference *c* is 0.015 arcsec.

5. CONCLUSIONS

We have taken advantage of the coherent nature of starlight to explore methods of adaptive optics in the near infrared applicable to any telescope, including dilute aperture arrays, which will be of particular benefit to future large telescopes. The MMT adaptive optics system has been used to achieve integrated images with resolution in one dimension better than 0.1 arcsec. The system is extremely versatile in that many different algorithms may be tested with a minimum of effort, which will allow direct comparison on such issues as speed, accuracy, and signal-to-noise. We will continue to pursue interferometric techniques for wavefront sensing with natural starlight, in particular the neural net and Fourier transform, both separately and in combination with CCD tilt sensing.

6. ACKNOWLEDGEMENTS

We thank Thermo Electron Technologies Corp. for donation of the adaptive mirror. Funds for the transputer wavefront computer were provided by the Flintridge Foundation. Infrared camera development and operation were funded by the NSF under grant AST-8822465. We recognize the invaluable contribution made by the late Dick Young in constructing the adaptive instrument. Observations reported here were made at the Multiple Mirror Telescope Observatory, a joint facility of the Smithsonian Institution and the University of Arizona.

7. REFERENCES

1. Angel, J.R.P., Wizinowich, P., Lloyd-Hart, M., & Sandler, D., *Nature*, **348**, 221-224, 1990.
2. Fugate, R.Q., Fried, D.L., Ameer, G.A., Boeke, B.R., Browne, S.L., Roberts, P.H., Ruane, R.E., Tyler, G.A., & Wopat, L.M., *Nature* **353**, 144-146, 1991.
3. Primmerman, C.A. Murphy, D.V., Page, D.A., Zollars, B.G., & Barclay, H.T., *Nature* **353**, 141-143, 1991.
4. Wizinowich, P., McLeod, B., Lloyd-Hart, M., Angel, R., Colucci, D., Dekany, R., McCarthy, D., Wittman, D., & Scott-Fleming, I., *Appl. Opt.*, in press.
5. Lloyd-Hart, M., Wizinowich, P., McLeod, B., Wittman, D., Colucci, D., Dekany, R., McCarthy, D., Angel, R., & Sandler, D., *Astrophys. J. Lett.*, in press.
6. Wizinowich, P., Lloyd-Hart, M., McLeod, B., Colucci, D., Dekany, R., Wittman, D., Angel, R., McCarthy, D., Hulburd, B., & Sandler, D., *Proc. Soc. Photo-Opt. Instrum. Eng.* **1542**, 148-158, 1991.
7. McCarthy, D.W., McLeod, B.A., & Barlow, D., *Proc. Soc. Photo-Opt. Instr. Eng.* **1237**, 496-507, 1990.
8. Hege, E.K., Diffraction-Limited Imaging with Very Large Telescopes, eds D.M. Alloin & J.-M. Mariotti, 141-155, Kluwer Academic, Dordrecht, 1989.
9. Sandler, D.G., Barrett, T.K., Palmer, D.A., Fugate, R.Q., & Wild, W.J., *Nature* **351**, 300-302, 1991.
10. Lippmann, R.P., *IEEE Acoustics, Speech, and Signal Processing Mag.*, 4-22, April 1987.
11. Rumelhart, D.E., Hinton, G.E., & Williams, R.J., in *Parallel Distributed Processing* Vol. 1, eds Rumelhart, D.E., & McClelland, J.L., MIT Press, Cambridge, 1986.
12. Lloyd-Hart, M., *Ph. D. Thesis* University of Arizona, Tucson, 1992.
13. Chaffee, F.H. & Cromwell, R.H., *Proc. Soc. Photo-Opt. Instr. Eng.* **1236**, 13-17, 1990.